

Tunneling magnetoresistance in Co-ZrO₂ granular thin films

B. J. Hattink, M. García del Muro, Z. Konstantinović, X. Batlle, and A. Labarta

Departament de Física Fonamental, Universitat de Barcelona, Avinguda Diagonal 647, 08028 Barcelona, Spain

M. Varela

Departament de Física Aplicada i Òptica, Universitat de Barcelona, Avinguda Diagonal 647, 08028 Barcelona, Spain

(Received 10 January 2005; revised manuscript received 19 October 2005; published 18 January 2006)

Granular films composed of well defined nanometric Co particles embedded in an insulating ZrO₂ matrix were prepared by pulsed laser deposition in a wide range of Co volume concentrations ($0.15 < x < 0.43$). High-resolution transmission electron microscopy (TEM) showed very sharp interfaces between the crystalline particles and the amorphous matrix. Narrow particle size distributions were determined from TEM and by fitting the low-field magnetic susceptibility and isothermal magnetization in the paramagnetic regime to a distribution of Langevin functions. The magnetic particle size varies little for Co volume concentrations $x < 0.32$ and increases as the percolation limit is approached. The tunneling magnetoresistance (TMR) was successfully reproduced using the Inoue-Maekawa model. The maximum value of TMR was temperature-independent within 50–300 K, and largely increased at low T , suggesting the occurrence of higher-order tunneling processes. Consequently, the tunneling conductance and TMR in clean granular metals are dominated by the Coulomb gap and the inherent particle size distribution.

DOI: [10.1103/PhysRevB.73.045418](https://doi.org/10.1103/PhysRevB.73.045418)

PACS number(s): 61.82.Rx, 68.55.-a, 74.25.Ha

I. INTRODUCTION

The enormous amount of research effort during the last 50 years on the magnetic behavior of nanostructured systems consisting of small particles is a sign of its continuing technological and scientific interest.¹ In particular, granular films with a very well controlled nanostructure have very promising technological applications as a result of technological advances in several film preparation techniques. From a scientific point of view, these technological advances make possible to prepare model granular solids with well controlled particle size and shape, thereby facilitating interpretation of their properties. Nevertheless, the behavior of these materials is determined by a complex interplay of intrinsic properties, size distribution of the nanoparticles, finite-size and surface effects, and many-body effects associated with interparticle interactions.^{2–6}

Finite-size effects dominate the magnetic behavior of individual nanoparticles, increasing their relevance as the particle size decreases. Among these, the phenomenon of superparamagnetism has probably provoked the largest amount of research. At low concentrations, the blocking of the magnetization of each particle is expected to occur at low enough T , this process becoming a collective phenomenon at high concentrations for which the freezing of the whole system of magnetic moments due to interparticle interactions is observed. However, there are still some open questions, e.g., the influence of the particle microstructure on the magnetization reversal. The superparamagnetic limit has relevant implications in the thermal and time stability of the bit in magnetic recording media.^{7,8}

Spin-dependent scattering in magnetic heterogeneous systems has also been the object of intense research in the past years since the discovery of giant magnetoresistance effect (GMR) in magnetic multilayers,⁹ granular alloys,^{10,11} magnetic tunnel junctions,^{12,13} and granular solids composed of

nanometric ferromagnetic (FM) particles in an insulating matrix (granular FM metals).^{14–18} In the dielectric regime, granular FM metals show giant tunneling magnetoresistance, caused by spin-dependent tunneling of the conduction electrons at the magnetic-insulator interfaces. Electrons with spin parallel to the particle magnetization have larger probability for tunneling than those electrons with antiparallel spin, leading to an overall lower resistance when all magnetic particle moments are aligned than in the case of randomly orientated moments. This magnetoresistive effect in granular materials is directly affected by magnetic correlations, since the latter determine the magnetic configuration of the system and, consequently, the magnetotransport properties. The T dependence of TMR and its value at low T are still under discussion in granular metals.^{19–24} Some results indicate that tunneling magnetoresistance (TMR) is almost temperature independent in a wide temperature range, in agreement with the Inoue-Maekawa model.²⁵ However, the relation between magnetism and magnetotransport in granular metals is still an open question, since there are systems showing strong temperature dependence of TMR.^{19,26,27} Some of these examples show the distinctive $1/T$ decay of TMR of the Helman-Abeles model.²⁰ Moreover, it is well known that imperfect metal-insulating interfaces and spin-flip scattering, due to, e.g., surface spin disorder and paramagnetic spins in the matrix, lead to an additional temperature decrease in TMR.

In the Helman-Abeles model, it is assumed that magnetic exchange energy has to be added to the Coulomb charging energy in order to account for TMR, so that these two energies are comparable. In contrast, Inoue and Maekawa²⁵ assume that the tunneling conductance in the dielectric regime can be derived from the classical expression for the spin-dependent tunneling in FM/I/FM junctions given by Landauer²⁸ and Maekawa and Gäfvert.²⁹ Inoue and Maekawa neglected the exchange energy as being small

when compared to the Coulomb energy. TMR is then temperature independent. We note that the experimental Coulomb energies are very high, for example in Co-Al-O samples with a high degree of intermixing (from 1.6 to 19 meV in Ref. 24), such that the Coulomb gap contributes to the overall resistance up to room temperature. In contrast, samples showing $1/T$ behavior of TMR display much lower values of the Coulomb energy (about 0.29 meV in Ref. 19 and 0.1 meV in Ref. 27; the exchange energy was about 0.31 meV in Ref. 19).

Besides, there is the open question of the strong increase of TMR at low temperature²⁴ which was not predicted by any of the two models, and needed the occurrence of higher-order tunneling processes. Granular solids display a broad particle size distribution such that the gross simplification of the Inoue-Maekawa model²⁵ is not to take into account tunneling between grains of different sizes. Mitani *et al.*²⁴ extended the model by assuming that the natural consequence of the particle size distribution is the successive onset, as the temperature is decreased, of tunneling processes between large grains through small ones. Mitani *et al.*²⁴ referred to these processes as “higher order” since they involve more than two particles. These processes are negligible at high temperature, where tunneling takes place through particles of similar sizes: electrons cannot tunnel either to a smaller particle, since the Coulomb charging energy is larger, or to a larger particle, which is further away, since the tunnel resistance is larger. This was already noted by Abeles *et al.*⁴

In this paper, we present a study of the magnetic and magnetotransport properties of granular Co-ZrO₂ thin films prepared by pulsed laser deposition (PLD) within a wide volume concentration range of Co ($0.15 < x < 0.43$). The samples display well defined Co nanoparticles and sharp particle-matrix interfaces. The size distribution of magnetic nanoparticles deduced from magnetic measurements is in a good agreement with the observation from high-resolution transmission electron microscopy (TEM) and allows us to fit the T and H dependences of the tunneling magnetoresistance (TMR). The particles are uniform in size almost for all Co concentrations and they are very small until percolation where big Co aggregates begin to appear. This is probably a consequence of the PLD used in the preparation of the samples. Finally, the maximum value of TMR is mostly T independent, except for very low T , at which it increases, suggesting the onset of higher-order tunneling process.

Our work suggests that tunneling conductance in clean granular metals is dominated by the Coulomb gap and that the higher-order tunneling processes between large particles mediated by small particles are intrinsic of granular metals, due to the inherent particle size distribution.

II. EXPERIMENTAL DETAILS

Co-ZrO₂ granular films were grown by KrF pulsed laser deposition (wavelength of 248 nm, pulse duration of $\tau = 34$ ns). The samples were deposited at room temperature in a vacuum chamber with rotating composite targets made of sectors of ZrO₂ and pure cobalt. Different surface ratio of target components led to different volume fraction x of Co,

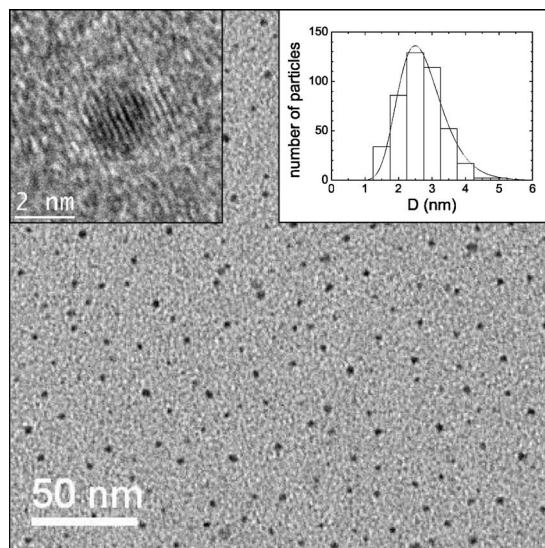


FIG. 1. TEM images of Co-ZrO₂ granular films with $x=0.20$. Left-hand-side inset shows the magnification of one particle. Right-hand-side inset shows the histogram of the size distribution obtained from the TEM micrograph. The solid line is the fit to a logarithmic-linear distribution.

ranging from metallic to dielectric regime ($0.15 < x < 0.43$). The distance between target and substrate was fixed at 30 mm. The laser fluency was typically 2 J/cm^2 .

Average compositions were determined by microprobe analyses. The films were structurally characterized with x-ray diffraction (XRD) and high-resolution transmission electron microscopy (TEM) (Fig. 1). The particle size distributions were also obtained by fitting the low-field magnetic susceptibility (zero-field cooling) (Fig. 2) and high-temperature isothermal magnetization curves $M(H)$ (Fig. 3) to a distribution of Langevin functions which model the superparamagnetic behavior of the particle size distribution.

The substrates for TEM experiments were silicon nitride membrane windows allowing observation of as-deposited samples. As an example, Fig. 1 shows a bright field TEM image of Co-ZrO₂ thin film with $x=0.20$. The dark regions indicate the Co particles and the light regions, the amorphous ZrO₂ matrix. The image clearly shows the presence of a regular distribution of Co grains. The particles have very well defined interfaces with the matrix. The left-hand-side inset to Fig. 1 shows a magnification of one particle. The lattice fringes observed in the grains correspond to Co atomic planes, which indicate that the grains are crystalline. The lattice fringes are not present in the ZrO₂ matrix, which suggests that the matrix is amorphous. The size distribution of the particles from TEM (right-hand-side inset to Fig. 1) has been fitted to a linear-logarithmic function with a mean particle size of $D=2.5$ nm and a width of $\sigma=0.25$ (solid line).

In a zero-field-cooled (ZFC) experiment, the sample is initially at a high temperature. Then the sample is cooled down to the lowest measuring temperature, a small magnetic field (typically 100 Oe) is applied, and the magnetization is measured as temperature is increased. The field-cooled (FC) experiment is similar, but a magnetic field is applied at a

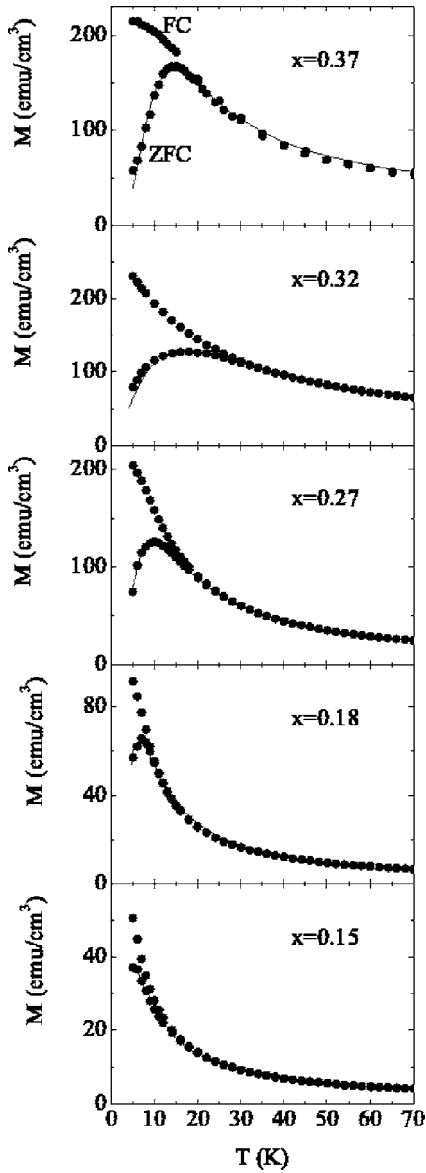


FIG. 2. Temperature dependence of the ZFC and FC magnetization of films with various Co concentrations (circles). Solid lines are the fits of ZFC curves to a distribution of Langevin functions, given by Eq. (1).

high temperature and the sample is cooled under the applied magnetic field. The magnetization curves $M(H)$ were recorded up to 50 kOe.

Magnetoresistance (MR) measurements were carried out by a four-probe technique using a lock-in amplifier and an ac constant current source at very low frequencies (57 or 111 Hz). The magnetoresistance curves $MR(T, H) = R(H, T) - R(H=0, T)$, being $R(H, T)$ the H - and T -dependent resistance, were measured within 30–300 K and up to either 10 or 50 kOe. The films prepared for transport measurements were deposited onto insulating glass substrates. After deposition, four parallel copper strips were evaporated on the sample surface. The strips were approximately 1 mm wide, and were separated by a distance of 0.7 mm in order to minimize the direct (geometric) electrode contribution to the capacitance.

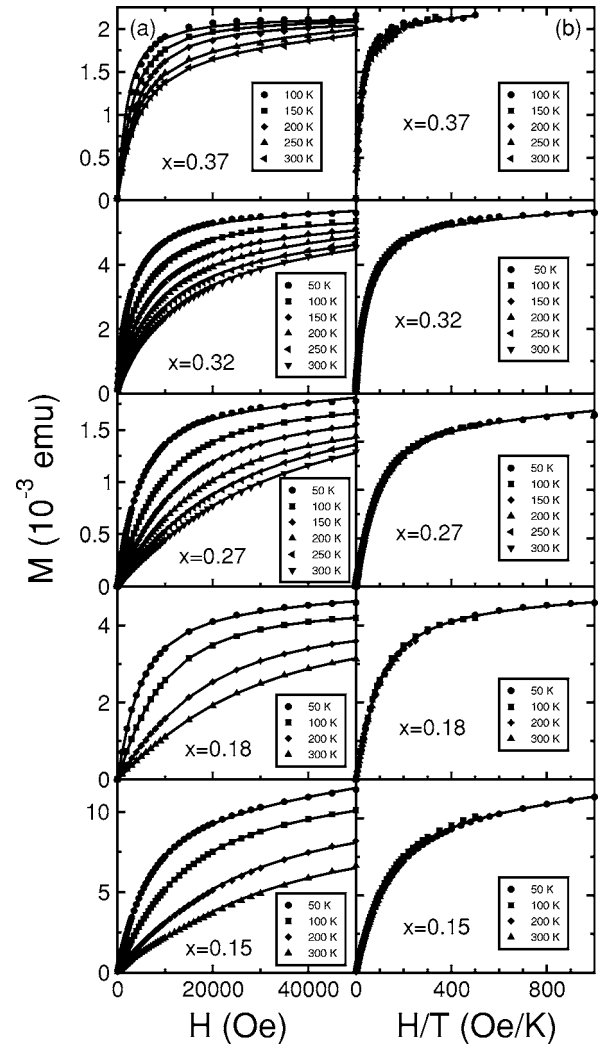


FIG. 3. (a) Field dependence of magnetization at different temperatures of films with various Co concentrations (circles). (b) Magnetization as a function of the reduced field H/T . The solid lines represent the fits to Eq. (2).

III. RESULTS AND DISCUSSION

A. dc susceptibility

The ZFC and FC curves of samples with different Co volume concentration well within the dielectric regime ($0.15 < x < 0.37$) are shown in Fig. 2 (circles). All the curves exhibit the characteristic features of a narrow distribution of small particles. The ZFC peak at the temperature T_p is observed at low temperatures for all concentrations, indicating a small mean particle size. The ZFC peak position moves from $T_p = 5$ K for $x = 0.15$ to 18 K for $x = 0.32$, which is a sign of a slight increase of the mean particle volume, as the Co volume concentration rises. From the values of T_p , the average anisotropy energy barrier $\langle KV \rangle$ can be estimated as $\langle KV \rangle \approx \ln(t/\tau_0)k_B \langle T_B \rangle$, where k_B is the Boltzmann constant, $\langle T_B \rangle$ is the mean blocking temperature, which is directly proportional to T_p ($T_p = \alpha T_B$, $\alpha = 2$ for a broad distribution³⁰), t is the time window (typically $t \approx 6$ s for the superconducting quantum interference device measurements) and τ_0 is the

TABLE I. Experimental values of T_p , T_{rev} , the average energy barrier $\langle KV \rangle$, Curie-Weiss constant C , and θ and parameters D_0 , σ , α_B obtained by fitting the ZFC curves in Fig. 2 for various Co concentrations.

x	T_p (K)	T_{rev} (K)	$\langle KV \rangle (10^{-14} \text{ erg})$	C (K)	Θ (K)	D_0 (nm)	σ	α_B (nm ³ /K)
0.15	5	12	1.9	280	0.3	1.3	0.16	0.9
0.18	7	13	2.6	460	-2.4	1.4	0.16	0.9
0.27	11	25	4.1	1700	-1.8	1.6	0.18	1.0
0.32	18	36	6.7	4900	7.0	1.8	0.24	1.0
0.37	15	42	5.7	3800	4.0	2.4	0.15	1.9

mean time between consecutive attempts to overcome the energy barrier which is about $\tau_0 \approx 10^{-11}$ s. The values for T_p and $\langle KV \rangle$ are given in Table I.

Above T_p , the ZFC and FC curves join at $T=T_{\text{rev}}$, i.e., T_{rev} stands for the T above which the $M(T)$ dependence becomes reversible (Table I). In this regime, the temperature dependence of the low-field susceptibility $\chi=M/H$ is given by the Curie-Weiss law $\chi(T)=C/(T+\theta)$. The value of C increases when the ferromagnetic concentration is increased, as expected for particles that become slightly larger as x increases, approaching the percolation threshold in the range $x_p \sim 0.45$ (Table I). The Curie-Weiss temperature θ is almost zero for $x \leq 0.27$, indicating negligible interactions between particles. The θ values for both $x=0.32$, 0.37 have a positive sign, which suggests dominant antiferromagnetic character of the interparticle interactions. Table I also summarizes the values of C and θ .

For temperatures below T_p , the FC curve keeps rising steeply except for the highest concentration $x=0.37$. Even for this concentration, the FC curve does not become completely flat, as has been observed for similar concentrations in Co-SiO₂ granular films¹⁵ and in metallic CoFe-Ag alloys.^{31,32} This feature seems to indicate the absence of strong magnetic interactions between particles for Co concentrations up to about $x=0.30$, as may also be deduced from the relatively small values of θ . Sankar *et al.*³³ reported $\theta = -29$ K and $\theta = -34$ K for Co-SiO₂ granular films with $x = 0.32$ and $x = 0.41$, respectively. These values are opposite in sign and much larger than the ones we found and may be related to stronger interactions in granular Co-SiO₂ than in Co-ZrO₂, which support the suggestion of our samples being clean samples with a very reduced degree of particle-matrix intermixing.

Experimental ZFC magnetization curves have been fitted (solid line in Fig. 2) to a distribution of Langevin function ($L(x)=\tanh^{-1}(x)-1/x$) with a temperature-dependent cut-off which models the blocking of the superparamagnetic behavior of the Co particles as the temperature is reduced:

$$M(H, T) = M_S \int_0^{D_B} L(M_S V H / k_B T) f(D) dD + M_{\text{res}}, \quad (1)$$

where V is the particle volume and H is the applied magnetic field. It was assumed that all particles have the bulk value for M_S ($M_S = 0.15 \mu_B / \text{\AA}^3$, where μ_B is the Bohr magneton). The particles are considered to have a linear-logarithmic size distribution $f(D)$, where D is the particle diameter. The thresh-

old diameter D_B and the blocking temperature T_B are directly related according to $D_B^3 = \alpha_B T_B$, where α_B is a fitting parameter [$2.5 < \alpha_B < 3.5 \text{ nm}^3/\text{K}$ for Co (Ref. 34)]. M_{res} accounts for any temperature-independent magnetization that may arise from ferromagnetic impurities (droplets) and/or diamagnetic contribution from the substrate or sample holder. The contribution of the blocked particles (particles with diameters $D > D_B$) has been neglected, since the ZFC curves were measured under a low magnetic field.

In all cases, a good agreement is achieved between the experimental data and the theoretical curves. The average particle diameter, $D_m = D_0 \exp(\sigma^2/2)$, is for small values of σ such as those listed in Table I, almost equal to D_0 . The fitting parameters, summarized in Table I, demonstrate that the average particle size is almost constant up to $x \sim 0.32$. The distribution width σ seems to become slightly larger for higher x with the exception of the $x=0.37$ sample, which appears to have a quite narrow size distribution. This is the reason why $x=0.32$ exhibits a higher T_p as compared to $x=0.37$ (Fig. 2). We note that the estimation of the average particle size from magnetic data requires the aprioristic assumption of the Co magnetization (per unit volume), which is usually taken as the bulk value (as it is done in our case). However, it is well known that the bulk value is an overestimation of the particle magnetization in fine particle systems, due to strong surface and finite-size effects.^{34,35} In our case, around 50–60 % of Co atoms are affected by the low-coordination number at the surface, giving rise to smaller M_S as compared to bulk Co. Consequently, this method leads to an underestimation of the average particle size^{34,35} as compared to that obtained from TEM.

The observed mean particle diameters are smaller and their growth with increasing concentration is less pronounced as compared to the data reported by Abeles and coworkers in co-sputtered Ni-Al₂O₃ (D varies from 1.5 nm for $x=0.08$ to 4 nm for $x=0.44$) and Ni-SiO₂ ($D=3.5$ nm for $x=0.40$) granular systems,^{30,36} the findings of Kodama *et al.* in sequentially sputtered Co-Al₂O₃,³⁷ and those of Sankar *et al.* in co-sputtered Co-SiO₂.^{15,33} This may be related to the choice of the matrix oxide: the ZrO₂ seems to coat the Co nanoparticles well confining them in small globules, thereby avoiding the growth of large clusters. The fact that our films have been prepared by means of laser ablation and not with the usual cathode sputtering may also explain the observed different microstructure, although similar sizes and concentration dependences have also been observed in co-sputtered Co-AlO_x films by Ohnuma and co-workers, who reported an average particle diameter of about 2 nm almost independent

TABLE II. Parameters D_0 , σ obtained by fitting the magnetization curves in Fig. 3, also as the effective anisotropy constants K and mean volume $\langle V \rangle$ for various Co concentrations.

x	D_0 (nm)	σ	$\langle V \rangle (10^{-21} \text{ cm}^3)$	$K (10^6 \text{ erg/cm}^3)$
0.15	1.3	0.18	1.2	16
0.18	1.4	0.18	1.4	18
0.27	1.6	0.17	2.1	20
0.32	1.8	0.23	3.6	19
0.37	2.4	0.17	7.2	8

of the Co concentration in a range from 20 up to 50 at. %.³⁸ We note that our results are also in accordance with other works on systems containing (various) discontinuous (less than one monolayer) Co layers embedded in Al₂O₃.^{39,40}

B. Magnetization

The magnetization as a function of the applied field for several Co concentrations and various temperatures in the superparamagnetic regime is given in Fig. 3(a). As in the case of ZFC curves, $M(H)$ can be fitted [solid line in Fig. 3(a)] to a distribution of Langevin functions as

$$M(H) = M_S \int_0^\infty L(M_S V H / k_B T) f(D) dD + \chi_{\text{res}}(T) H. \quad (2)$$

The last term in Eq. (2) corresponds to a residual susceptibility, which is necessary to account for paramagnetic and/or diamagnetic residual contributions, coming essentially from the substrate and the matrix. Equation (2) is valid in the superparamagnetic regime, i.e., for temperatures well above the blocking temperature. Equation (2) points out that the magnetization only depends on the reduced parameter H/T , as long as the last term has been subtracted from experimental data. This implies that in the superparamagnetic regime the magnetization curves should scale when M is plotted as a function of H/T . We observe that the magnetization curves scale for $x \leq 0.37$ [Fig. 3(b)]; a fact which confirms the absence of any significant interparticle interactions for these concentrations.

It is worth noting that the magnetic behavior of the samples becomes increasingly softer as the Co content increases, which should be a direct consequence of the growth in size of the Co particles observed as x increases. However, the particle diameters are quite similar for all concentrations and, only close to percolation, large aggregates start to form leading to an overall increase of the mean particle size.

The width of the particle-size distribution obtained from the fit of $M(H)$ to Eq. (2) becomes gradually broader as Co fraction increases (see Table II). It should be noted though, that the sample with $x=0.37$ displays a somewhat different behavior: it seems to have a narrower particle size distribution in spite of its relatively higher Co content, which manifests itself in a more Langevin-like $M(H)$ dependence. On the other hand, those samples with a large σ exhibit a steeper rise in $M(H)$ for low fields as well as a slower but steadier increase for high magnetic fields. As we have already noted

for the ZFC curves, the actual preparation conditions (energy and fluency of the beam, substrate position, etc.) produce some variation in the mean particle size and width of the distribution, even for samples with close nominal Co contents. The microstructure of the samples thus depends to some extent on the synthesis conditions.

It is worth noting that the fitted particle size distributions (Table II) are in perfect agreement with those values found by fitting ZFC curves. Using these diameters and the $\langle KV \rangle$ values from Table I, the effective anisotropy constant K can be estimated (see Table II). The anisotropy constant is fairly constant ($K \sim 16\text{--}20 \text{ erg/cm}^3$) for all concentrations except for $x=0.37$ for which is significantly smaller ($K \sim 8 \text{ erg/cm}^3$).

For bulk fcc Co, the effective magnetocrystalline anisotropy constant is given by $K_{\text{eff}} = K_1/4$,^{30,41} where K_1 is the first-order anisotropy constant whose value is approximately $K_1 \approx 2.6 \times 10^6 \text{ erg/cm}^3$ for Co.^{42,43} This leads to $K_{\text{eff}} \approx 6.5 \times 10^5 \text{ erg/cm}^3$. In comparison to this value, our values of K are larger, strongly suggesting that surface anisotropy gives an additional contribution for such small particles and raises the total effective anisotropy. Luis *et al.*⁴⁰ recently reported a size-dependent effective anisotropy constant of sputtered Co cluster in Al₂O₃ that went down from $2.4 \times 10^7 \text{ erg/cm}^3$ for $\langle D \rangle = 0.8 \text{ nm}$ to $3 \times 10^5 \text{ erg/cm}^3$ for $\langle D \rangle = 5.2 \text{ nm}$ and showed a linear dependence on the logarithm of the mean diameter. Jamet *et al.*³⁴ report a slightly smaller effective anisotropy constant of $2 \times 10^6 \text{ erg/cm}^3$ for Co particles with a 3-nm diameter in a niobium matrix. Our results are in good agreement with these experimental findings.

From the volume anisotropy K of the nanoparticles and that of their bulk counterpart K_V , the value of surface anisotropy K_S can be estimated for spherical particles¹ with diameter D , as $K = K_V + (6/D)K_S$. Taking $K \sim 18 \times 10^6 \text{ erg/cm}^3$, $D \sim 1.5 \text{ nm}$ and $K_V \sim 6.5 \times 10^5 \text{ erg/cm}^3$, we obtain $K_S \sim 0.43 \text{ erg/cm}^2$, which is in agreement with previous results for Co ($K_S \sim 0.2\text{--}0.4 \text{ erg/cm}^2$ in Ref. 44) and other nanoparticle systems.³⁵

C. Magnetoresistance

In the dielectric regime, the temperature dependence of the dc resistivity follows an exponential decay with $T^{-1/2}$ for all samples below the percolation threshold,^{45,46} which is characteristic of insulating granular systems with a distribution of nanometric particle sizes in which conduction takes place by thermally assisted tunneling.⁴

The field dependence of the tunneling magnetoresistance (TMR) of a Co-ZrO₂ sample with $x=0.34$ is plotted in Fig. 4(a). Figure 4(b) displays a zoom for low fields, which shows a finite coercive field H_C of about 300 Oe at 10 K. These features correlate with the $M(H)$ behavior, as shown in Figs. 4(c) and 4(d). The maximum of the resistance-field $R(H)$ curve takes place at the coercive field, which corresponds to the state of maximum disorder in the orientation of the neighboring magnetic particle moments. Therefore the field dependence of the resistance, which is related to the alignment between particle moments, reaches a maximum. We also observe that for high fields ($H > 10 \text{ kOe}$) the resis-

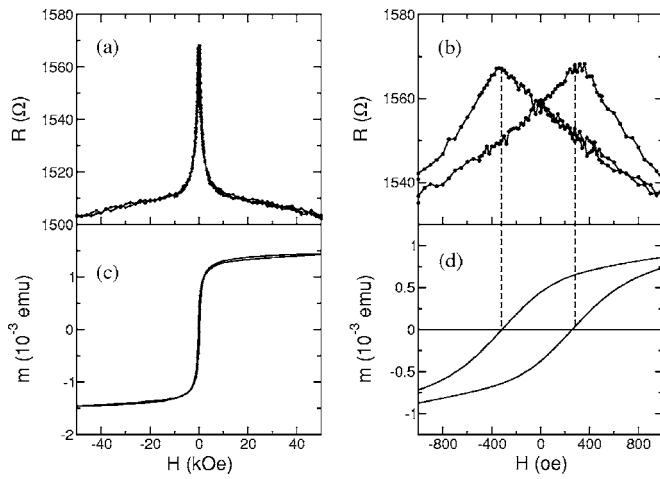


FIG. 4. (a) Magnetoresistance and (c) magnetization of a Co-ZrO₂ sample with $x=0.34$ at 10 K. (b) and (d) shows the low-field behavior.

tance keeps decreasing with an almost linear field dependence. This high-field magnetoresistance is probably caused by some spin disorder at the particle-matrix interfaces, which are magnetically very hard, and/or any residual magnetic impurities inside the oxide matrix.

In Figs. 5(a)–5(c), we show magnetoresistance curves at different temperatures and for several Co concentrations (circles). All samples exhibit a negative tunneling magnetoresistance, typical of a system consisting of small magnetic particles. As in the case of the magnetization, the magnetoresistance drop becomes much more abrupt at low temperatures, in accordance with the temperature dependence observed in the magnetization curves (Fig. 3). A maximum magnetoresistance of about 7% at 50 kOe, which is almost temperature independent, is reached for a concentration around $x=0.37$, in very close agreement with $\text{TMR} \sim 6.8\%$ at 77 K for Co₃₈(SiO₂)₆₂.¹⁵ Sankar *et al.*¹⁵ argue that a T -independent value of the magnetoresistance is due to reduced intermixing and negligible spin flipping. The magnetoresistance diminishes for very low and high Co concentrations and vanishes completely when the percolation threshold is reached, as expected.¹

The MR curves, in the superparamagnetic regime, have been fitted to the expression²⁵ $\text{TMR} = P^2 m^2 / (1 + P^2 m^2)$, where P is polarization of the Co tunneling electrons, $m = M(H)/M_s$ is the reduced magnetization of the system and M_s is the saturation magnetization. In this expression, m can be replaced by the integral over all particle diameters of the Langevin function $L(H, T) = L(M_s V H / k_B T)$:

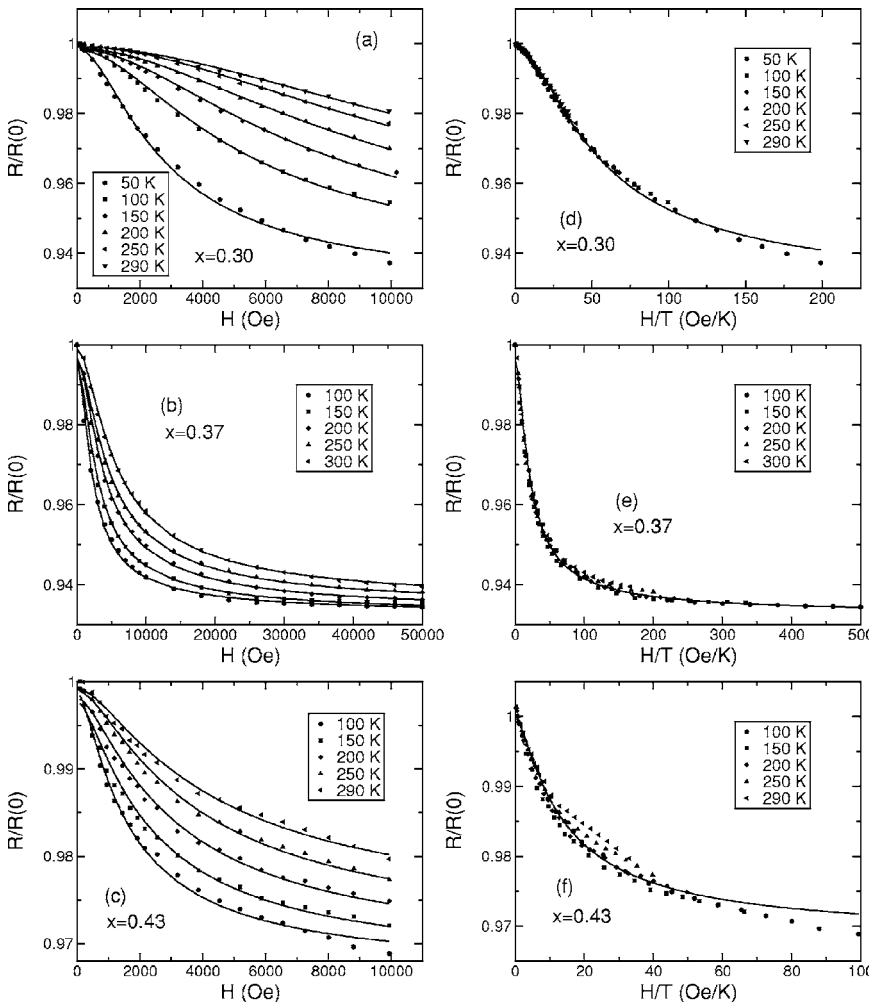


FIG. 5. (a)–(c) Field dependence of magnetoresistance at different temperatures of films with several Co concentrations (circles). (d), (e) Same data plotted as a function of H/T . Solid lines are fits to Eq. (3).

TABLE III. Parameters D_0 and σ used to fit the magnetoresistance curves in Fig. 5.

x	D_0 (nm)	σ
0.25	1.9	0.36
0.37	2.7	0.17
0.43	2.9	0.28

$$m(H,T) = \int_0^{\infty} f(D)L(H,T)dD, \quad (3)$$

where $f(D)$ is the linear-logarithmic distribution function. The values of the fitting parameters D_0 and σ are listed in Table III. If the proposed model were to be valid, the magnetoresistance curves corresponding to different temperatures should scale in a unique master curve when plotted as a function of H/T , since the field and temperature dependence enter in Eq. (3) through the Langevin function $L(H,T)$. At low Co concentrations, the MR curves [Figs. 5(d)–5(f)] indeed scale fairly well, while for $x=0.43$ the scaling becomes worse, indicating that the field dependence of the magnetoresistance starts to deviate from Eq. (3) due to magnetic interactions between particles, as we approach the percolation threshold. However, even for these relatively high concentrations, the fitting is still acceptable giving rise to reasonable values of the parameters.

The maximum of the magnetoresistance is almost temperature independent above about 100 K, as best shown in Fig. 5(b), in the panel corresponding to $x=0.37$. However, an enhanced MR is observed at low temperature (see Fig. 6). These observations are in accordance with Mitani *et al.*^{21,24} and Zhu *et al.*⁴⁷ in Co-AlO_x and Fe-AlO_x, respectively. Mitani and co-workers²⁴ explained their results in terms of the occurrence of higher-order tunneling processes between large particles mediated by small particles as T decreases, and fitted their experimental data to the equation

$$\text{TMR} = 1 - (1 + P^2 m^2)^{-(n^*+1)}, \quad (4)$$

where $n^* = (B/2\chi^* sT)^{1/2}$, $\chi^* = k\chi$, k being a constant defined in Ref. 24 and $\chi = \sqrt{2m^* \Phi / \hbar^2}$, Φ being the effective barrier height with respect to the Fermi level E_F , s being the separation between particles, and B being the prefactor in the well-known expression $R(T) = R_0 \exp[-(B/T)^{1/2}]$.⁴ The increase in the maximum MR at very low temperature has also been tentatively discussed in terms of the effect of the cluster-surface and matrix interactions leading to a dominant d character of the tunneling electrons.²³

Our experimental data have also been fitted to Eq. (4) (solid line in Fig. 6) using a spin polarization of $P=0.25 \pm 0.02$, $\chi^* s = 97 \pm 10$, and a barrier $B=25.3$ meV. The factor B was obtained from a linear regression of $\ln[R(T^{-1/2})]$ data,^{45,46} while the parameters P and $\chi^* s$ were chosen to fit the experimental data. We note that the obtained spin polarization $P=0.25$ coincides rather well with the value $P=0.27$ obtained by fitting the field dependence of the MR, and it is reasonable agreement with the experimental⁴⁸ ($P=0.35$) and theoretical⁴⁹ ($P=0.33$) values for Co. From the previous analysis, as the effect of intermixing and spin flipping are expected to be limited, the reduced values of P suggest the role of the insulating matrix in determining the actual value of P , as suggested by Slonczewski.⁵⁰ It is worth noting that the experimental results in Fig. 6 cannot be fitted to the $1/T$ behavior of the Helman-Abeles model (Ref. 20) in any temperature range.

At high temperature the experimental MR ratio diminishes a bit more rapidly as compared to the theoretical prediction. This behavior has also been observed in Co-AlO_x (Ref. 25) and Fe-Al₂O₃ (Ref. 47) granular thin films. Zhu and Wang⁴⁷ attributed this decrease of the magnetoresistance to spin-flip scattering processes due to magnetic impurities contained in the tunneling barriers.

IV. CONCLUSION

Magnetic properties and tunneling magnetoresistance of Co-ZrO₂ granular insulating thin films were measured in a series of samples with Co concentrations up to the percolation threshold. The particle size distribution obtained by fitting the low-field magnetic susceptibility, high-temperature isothermal magnetization, and TMR are in close agreement, and match direct TEM observations. The magnetic particle size varied little for Co concentrations $x < 0.32$, and the absence of strong magnetic interactions between particles was evidenced. As the percolation limit was approached, the particle diameter increased as a consequence of the formation of larger aggregates, favoring interparticle interactions. The magnetic anisotropy of the Co particles was approximately one order of magnitude higher than that of bulk fcc Co, which is related to the surface contribution to the total anisotropy. The maximum value of TMR was T independent above 50 K and followed the Inoue-Maekawa model, showing that Co-ZrO₂ granular thin films prepared by PLD lead to well-defined Co particles with sharp particle-matrix interfaces. The very high values of the exponent B in the

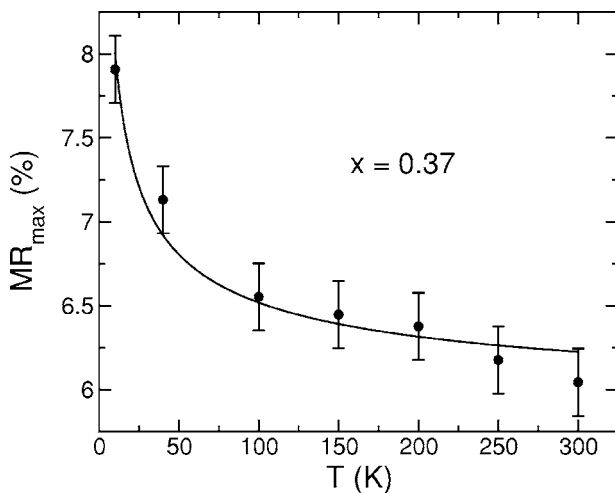


FIG. 6. Temperature dependence of the magnetoresistance of Co-ZrO₂ film with $x=0.37$ (circles). The solid line is the fit to Eq. (4).

temperature dependence of the resistance further supports the high quality of the particle-matrix interfaces in a very wide compositional range. This enables the occurrence of high Coulomb charging energies, so that the Coulomb gap dominates $R(T)$ up to almost room temperature and the magnetic exchange energy (in the Helman-Abeles model) is negligible. Consequently, TMR is almost temperature independent, except for the strong increase at low temperature, which

suggests that higher-order tunneling processes are intrinsic of granular metals, due to inherent particle size distribution.

ACKNOWLEDGMENTS

Financial support of the Spanish CICYT (Grant No. MAT2003-01124) and the Catalan DURSI (Grant No. 2001SGR00066) is gratefully recognized.

- ¹For a review, see X. Batlle and A. Labarta, *J. Phys. D* **35**, R15 (2002).
- ²C. L. Chien, *Science and Technology of Nanostructured Magnetic Materials*, edited by G. C. Hadjipanayis and G. A. Prinz (Plenum Press, New York, 1991), p. 477.
- ³C. L. Chien, *J. Appl. Phys.* **69**, 5267 (1991).
- ⁴B. Abeles, P. Sheng, M. D. Coutts, and Y. Arie, *Adv. Phys.* **24**, 407 (1975).
- ⁵B. Abeles, *Applied Solid State Science: Advances in Materials and Device Research*, edited by R. Wolfe (Academic, New York, 1976).
- ⁶C. L. Chien, J. Q. Xiao, and J. S. Jiang, *J. Appl. Phys.* **73**, 5309 (1993).
- ⁷C. Hancock, *J. Phys. D* **29**, 2343 (1996).
- ⁸L. He, *J. Magn. Magn. Mater.* **155**, 6 (1996).
- ⁹M. N. Baibich, J. M. Broto, A. Fert, F. Nguyen Van Dau, F. Petroff, P. Eitenne, G. Creuzet, A. Friederich, and J. Chazelas, *Phys. Rev. Lett.* **61**, 2472 (1988).
- ¹⁰A. E. Berkowitz, J. R. Mitchell, M. J. Carey, A. P. Young, S. Zhang, F. E. Spada, F. T. Parker, A. Hutten, and G. Thomas, *Phys. Rev. Lett.* **68**, 3745 (1992).
- ¹¹J. Q. Xiao, J. S. Jiang, and C. L. Chien, *Phys. Rev. Lett.* **68**, 3749 (1992).
- ¹²J. S. Moodera, L. R. Kinder, T. M. Wong, and R. Meservey, *Phys. Rev. Lett.* **74**, 3273 (1995).
- ¹³T. Miyazaki and N. Tezuka, *J. Magn. Magn. Mater.* **139**, L231 (1995).
- ¹⁴A. Milner, A. Gerber, B. Groisman, M. Karpovsky, and A. Gladkikh, *Phys. Rev. Lett.* **76**, 475 (1996).
- ¹⁵S. Sankar, A. E. Berkowitz, and D. J. Smith, *Phys. Rev. B* **62**, 14273 (2000).
- ¹⁶M. Holdenried and M. Micklitz, *Eur. Phys. J. B* **13**, 205 (2000).
- ¹⁷S. Mitani, H. Fujimori, and S. Ohnuma, *J. Magn. Magn. Mater.* **165**, 141 (1997).
- ¹⁸H. Fujimori, S. Mitani, and S. Ohnuma, *J. Magn. Magn. Mater.* **156**, 311 (1996).
- ¹⁹J. M. D. Coey, A. E. Berkowitz, Ll. Balcells, F. F. Putris, and A. Barry, *Phys. Rev. Lett.* **80**, 3815 (1998).
- ²⁰J. S. Helman and B. Abeles, *Phys. Rev. Lett.* **37**, 1429 (1976).
- ²¹S. Mitani, H. Fujimori, K. Takanashi, K. Yakushiji, J.-G. Ha, S. Takahashi, S. Maekawa, S. Ohnuma, N. Kobayashi, T. Masumoto, M. Ohnuma, and K. Hono, *J. Magn. Magn. Mater.* **198-199**, 179 (1999).
- ²²M. Holdenried, B. Hackenbroich, and H. Micklitz, *J. Magn. Magn. Mater.* **231**, 13 (2001).
- ²³B. Hackenbroich, H. Zare-Kolsaraki, and H. Micklitz, *Appl. Phys. Lett.* **81**, 514 (2002); H. Zare-Kolsaraki, B. Hackenbroich, and H. Micklitz, *Europhys. Lett.* **57**, 866 (2002).
- ²⁴S. Mitani, S. Takahashi, K. Takanashi, K. Yakushiji, S. Maekawa, and H. Fujimori, *Phys. Rev. Lett.* **81**, 2799 (1998).
- ²⁵J. Inoue and S. Maekawa, *Phys. Rev. B* **53**, R11927 (1996).
- ²⁶J. I. Gittleman, Y. Goldstein, and S. Bozowski, *Phys. Rev. B* **5**, 3609 (1972); J. I. Gittleman, B. Abeles, and S. Bozowski, *ibid.* **9**, 3891 (1974).
- ²⁷Ll. Balcells, J. Fontcuberta, B. Martínez, and X. Obradors, *Phys. Rev. B* **58**, R14697 (1998); Ll. Balcells, J. Fontcuberta, B. Martínez, and X. Obradors, *J. Phys.: Condens. Matter* **10**, 1883 (1998); Ll. Balcells, B. Martínez, F. Sandiumenge, and J. Fontcuberta, *ibid.* **12**, 3013 (2000).
- ²⁸R. Landauer, *Philos. Mag.* **21**, 863 (1970).
- ²⁹S. Maekawa and U. Gäfvert, *IEEE Trans. Magn.* **18**, 707 (1982).
- ³⁰J. I. Gittleman, B. Abeles, and S. Bozowski, *Phys. Rev. B* **9**, 3891 (1974).
- ³¹S. R. Teixeira, B. Dieny, A. Chamberod, C. Cowache, S. Auffret, P. Auric, J. L. Ruvière, O. Redon, and J. Pierre, *J. Phys.: Condens. Matter* **6**, 5545 (1994).
- ³²X. Batlle, V. Franco, A. Labarta, and K. O'Grady, *J. Appl. Phys.* **88**, 1576 (2000).
- ³³S. Sankar, D. Dender, J. A. Borchers, D. J. Smith, R. W. Erwin, S. R. Kline, and A. E. Berkowitz, *J. Magn. Magn. Mater.* **221**, 1 (2000).
- ³⁴M. Jamet, V. Dupuis, P. Mélinon, G. Guiraud, A. Pérez, W. Wernsdorfer, A. Traverse, and B. Bagnard, *Phys. Rev. B* **62**, 493 (2000).
- ³⁵X. Batlle, M. García del Muro, J. Tejada, H. Pfeiffer, P. Görnert, and E. Sinn, *J. Appl. Phys.* **74**, 3333 (1993).
- ³⁶P. Sheng, B. Abeles, and Y. Arie, *Phys. Rev. Lett.* **31**, 44 (1973).
- ³⁷R. H. Kodama and A. S. Edelstein, *J. Appl. Phys.* **85**, 4316 (1999).
- ³⁸M. Ohnuma, K. Hono, E. Abe, H. Onodera, S. Mitani, and H. Fujimori, *J. Appl. Phys.* **82**, 5646 (1997).
- ³⁹H. Graf, J. Vancea, and H. Hoffmann, *Appl. Phys. Lett.* **80**, 1264 (2002).
- ⁴⁰F. Luis, J. M. Torres, L. M. García, J. Bartolomé, J. Stankiewicz, F. Petroff, F. Fettar, J. L. Maurice, and A. Vaures, *Phys. Rev. B* **65**, 094409 (2002).
- ⁴¹C. P. Bean and J. D. Livingstone, *J. Appl. Phys.* **30**, 1205 (1959).
- ⁴²J. P. Chen, C. M. Sorensen, K. J. Klabunde, and G. C. Hadjipanayis, *Phys. Rev. B* **51**, 11527 (1995).
- ⁴³W. A. Sucksmith and J. E. Thompson, *Proc. R. Soc. London, Ser. A* **225**, 362 (1954).
- ⁴⁴V. Gradmann, *J. Magn. Magn. Mater.* **54-57**, 733 (1986).

- ⁴⁵B. J. Hattink, A. Labarta, M. Garcia del Muro, X. Batlle, F. Sánchez, and M. Varela, *Phys. Rev. B* **67**, 033402 (2003).
- ⁴⁶B. J. Hattink, M. García del Muro, Z. Konstantinovi, V. F. Puentes, X. Batlle, A. Labarta, and M. Varela, *Int. J. Nanotechnol.* **2**, 43 (2005).
- ⁴⁷T. Zhu and Y. J. Wang, *Phys. Rev. B* **60**, 11918 (1999).
- ⁴⁸R. Meservey and P. M. Tedrow, *Phys. Rep.* **283**, 173 (1994).
- ⁴⁹M. B. Stearns, *J. Magn. Magn. Mater.* **5**, 167 (1977).
- ⁵⁰J. C. Slonczewski, *Phys. Rev. B* **39**, 6995 (1989).